Digest Journal of Nanomaterials and Biostructures Vol. 17, No. 4, October-December 2022, p. 1345-1352

The effect of synergistic interaction of ceria-doped copper oxide prepared by hydrothermal method as toxic gas sensor

A. S. Mohammed*, S. O. Abdulghani
Ministry of Education, Direction of Education in AL-Anbar, Anbar, Iraq

The effect of introducing cerium oxide (CeO_2) at 5% and 9% concentrations as dopants to improve the catalytic performance of the copper oxide (CuO) nanoparticles was studied using a hydrothermal technique. The seed layer is placed in an autoclave, usually made of Teflon, and heated with water for 10 hours at 100°C. The resulting films were characterized using X-ray diffraction (XRD), atomic force microscopy (AFM), and photoluminescence (PL). The grain size decrease as the doping concentration increases, while the roughness, and RMS increase. The sensor was developed to detect different concentrations of ammonia (NH_3) gas. CuO at 9% of CeO_2 sample exhibited the highest sensitivity about (48%) for NH_3 gas at 1.5C.

(Received July 14, 2022; Accepted November 25, 2022)

Keywords: CuO, Hydrothermal, Gas sensor, Sensitivity, NH3

1. Introduction

Modern technological and manufacturing advancements result in increased amounts of toxic gases being emitted into the atmosphere, causing pollution of internal environments. of these gases are highly toxic and their presence, even in a few tens of parts per million, is a threat to human life. Therefore, extremely selective and sensitive detection of gases is required to monitor and control the quality of the environment [1]. Nano sensors can take advantage of the combination of four different advantages typical of nanostructure: Quantitative confinement effect (I), surface-to-volume ratio (II), NP shape and aggregation (III), and nanomaterial agglomeration state (IV). (the nanoparticle (NP) is used here to depict in general, any type of structure with at least one dimension in the nano range). Materials with nanostructures such as nanowires, nanotubes, and nanoballs improve the behavior of sensitive materials for operating devices at room temperature (RT) [2]. Metal oxide semiconductors (MOS) have a rich history of industrial and scientific achievements in the field of gas sensors, dating back to the 1950s and 1960s and continuing to the present day, and efforts are still continuing to provide the best. As early work emphasized leakage detection and safety applications, at present, applications seek to develop sensors to monitor indoor and outdoor air quality, with the aim of assorting selective gases and quantifying the concentrations of environmental pollutants [3]. Nanostructured metal oxide semiconductors are frequently used in the manufacture of sensors that can detect reducing and oxidizing gases like NH_3. MOS sensors have received a significant amount of attention due to their great stability, inexpensive, and flexibility with microelectronic technology [4]. Copper oxide (CuO) is one metal oxide semiconductor, which possesses a low band gap of about 1.2–2.0 eV and has a p-type conductivity [5]. CuO is the most researched copper oxide in terms of sensing applications because it is more stable than Cu_2O and Cu_2O_3, which are regarded as not viable materials for gas-sensing applications. It is stable when exposure to different gases, and comparatively low changes of standard resistivity were observed [6]. CuO and derived materials were previously tested to sense nitrogen oxide (NO_2), hydrogen sulfide (H_2S), ammonia (NH_3), carbon monoxide (CO), and ethanol (C_2H_5OH) at an operating temperature of 200–400°C [7]. The addition of ceria (CuO_2) impurities to copper oxide (CuO) has become a topic of interest due to its wide applications and its distinct properties such as reflectivity, transparency, and low electrical sheet resistance[8]. To our knowledge, ceria-doped copper oxide has not yet been used for NH3 detection by the hydrothermal method at room temperature. It is well known that the morphology,

* Corresponding author: baker.sabbar3@gmail.com
https://doi.org/10.15251/DJNB.2022.174.1345

grain size, structural, and chemical properties of any gas sensitive material used in resistivity sensors have a significant impact on their selectivity and performance of sensor, which enhance the chemisorption processes [9]. Cerium oxide, often known as ceria (CeO_2), is an important rare earth sensor material used to monitor environmental gases. It has several advantages, including strong chemical corrosion resistance, non-toxicity, safety, and reliability, and it has sparked a lot of interest as an NH_3 gas sensor, also [10]. It has a high oxygen storage capacity (OSC), a large number of oxygen vacancies, and a powerful interaction with metals. Moreover, the catalytic activity of CuO could be enhanced when doped with CeO_2, as a result of the reaction of ceria with copper ions [11]. Doping with metal ions has a synergistic impact. Metallic ion substitutional doping into the ceria oxide lattice, for example, can produce crystal lattice deformation, and thereafter the figuration of a new interface between jointly components. This synergistic action works in conjunction with the oxygen donation of ceria generated by partial Ce4+/Ce3+ reduction to increase the concentration of oxygen vacancies in the CuO bulk or on the surface, as well as the mobility of lattice oxygen. As a result, the Cu-O-Ce structure is formed, which plays an important role in the NH_3 oxidation process [12]. We focused on nanomaterials prepared in different sizes, with the help of ceria. The nanocrystal appears to be critical for a good enough sensor response. The aim of this paper is to devote more attention to studying the sensor structure of Ceria-doped CuO towards NH3 gas and the effect of rare earth element addition on the structural, optical and resistive behavior of CuO films.

2. Experimental work

In this paper 1.25 g of $CuCl_2.2H_2O$ used as a source of CuO, dissolved in 50 ml of deionized water to obtain a homogeneous blue-colored solution. For 60 minutes, the solution was constantly stirred. After that, 10 ml of an aqueous solution of NaOH is added, and the blend is put in the autoclave inside the oven at a temperature of 140°C for 2 hours, and then the solution is cooled to obtain a black precipitate. CeO_2 nanoparticles made from $Ce(SO_4)_2.4H_2O$ using the same method. Finally, a seed layer of CuO with various CeO2 doping concentrations (0.05, 0.09% wt.) is prepared on a glass substrate by the spin coating method for 30 seconds at 2000 rpm. The structure properties are examined using an X-ray diffractometer system (Philips PW 1710, X-ray diffractometer, USA). The morphological characterization of the produced films was tested using field emission electron microscopy (FESEM), Nova Nanosem 450, USA. Photoluminescence spectrometers were used to evaluate the optical characteristics of the deposited films by PL (model LS-50B). The sensor architecture is schematically depicted in (Fig. 1, a). By an Edwards thermal evaporation system (E306A), Aluminum (Al) vapor was deposited in a vacuum under a closed chamber pressure of 10^{-3} Pa.

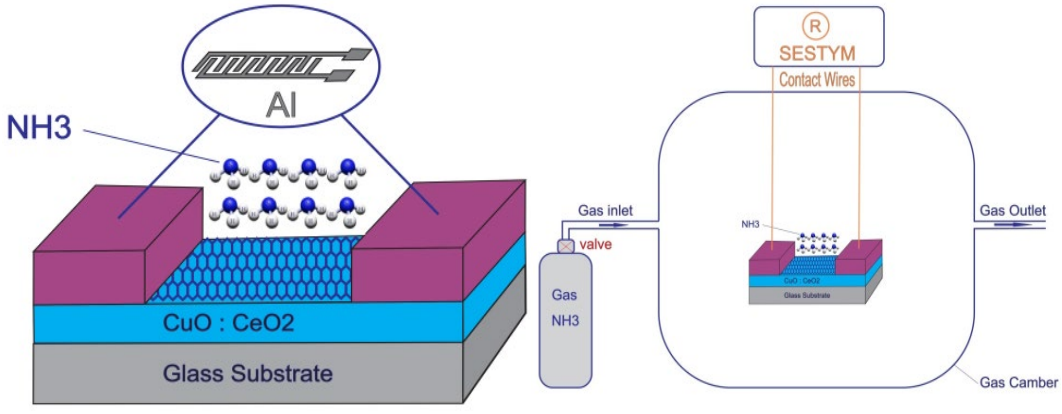

(a) *(b)*

Fig. 1. (a) Sensor structure and (b) measurement setup schematic illustration.

The prepared sensor was placed inside an airtight chamber (Fig. 1, b). Gas sensing performance was evaluated using a computer and a digital multimeter connected to a PC (UNI-TUT81B). The manufactured system was used to detect and record changes in sensor resistance caused by exposure to NH_3 gas.

3. Results and discussion

3.1. Structural properties

Fig. 2 displays X-ray analysis of pure CuO and CeO_2 doped CuO thin films at 5% and 9% ratios of CeO_2. The XRD results showed the formation of copper nanoparticles. According to the JCPDS file (card No. 05-0661), the diffraction peaks of the deposited films have a polycrystalline structure in nature and it is indexed as a monoclinic structure, which is consistent with the result of researcher Ahmed [13]. The diffraction peaks of 2θ = 35.5, 38.7, 48.7, and 61.6 are attributed to the (002), (111), (-202), and (-113) levels, these results are close to the researcher Zhang [12]. It turns out that the preferred level and greater intensity pattern for all deposited films is (002) because its crystals are generated with more periodicity than the other crystal patterns. In other words, in the case of symmetrical crystals, the rays are reflected with greater intensity in the pattern's direction (002), whereas in the case of random crystals, the strength of the diffraction pattern diminishes, as is observed with other patterns. The diffraction patterns indicated a slight difference in the d-spacing between the diffraction levels from the typical values, especially at the (-202) level. Defects in the crystal lattice cause a shift in the d-spacing between the diffraction levels. The inhomogeneity of stoichiometric transport causes crystal lattice defects. Moreover, the thermal stress due to the temperature of the substrate causes the lattice to contract or expand, and thus a shift in the angle of diffraction occurs [14]. When impurities are added, a new peak is evident at 5% concentration, indicating CeO2 atoms at 2θ = 33.078, (200) plane. The same figure shows an increase in the intensity of this peak, while the preferred CuO peak intensity decreases with an increase in the doping ratio. Also there are new peak appear at 2θ =28.5 at 9% of CeO2 concentration, which refer to plane (111) of the cubic structure, from the International Center for Diffraction(card no. 96-900-9009). The lowering in the ratio of intensity of the CuO diffraction peak with increasing doping concentration may be because of the saturation of new nuclei centers which are created by the impurity added [15], and, thus, the atoms of CeO_2 will become random material on the surfaces of the films. To compute the mean crystalline size from the FWHM of XRD lines, the Debye-Scherrer formula[16] is utilized.

$$D = K\lambda/\beta\, cos\theta \tag{1}$$

where K is the Scherrer constant, which is normally equal to 0.9, β is refere to FWHM is in radians, wavelength (λ) is in nanometers, and θ refere to diffraction angle is in radians. The results reveal that as the doping ratio and FWHM increase, the mean crystallite size of CuO drops from 23 to 19.4 and 18.1 nm, respectively.

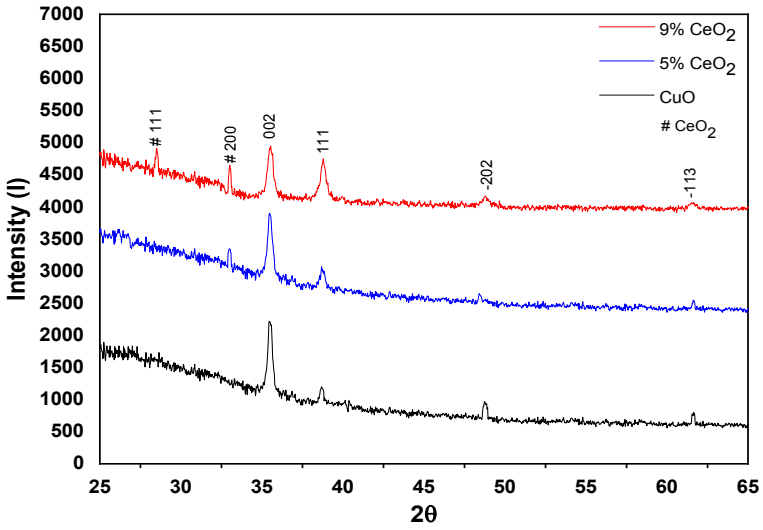

Fig. 2. X-ray of CuO and CeO_2-doped CuO at (5% and 9%) of CeO_2.

3.2. AFM Topography

The surface morphologies of the CuO and CeO_2 doped CuO thin films, as illustrated in Fig. 3, were studied using the atomic force microscopy (AFM) technique. The AFM images are displayed, and all of the samples shown have a granular structure. The image of pure CuO film displays a uniform distribution of densely packed grains. The average diameter of pure CuO film is 61.4 nm with more clarity (column-like) and decreases with increasing doping ratios. Table.1 revealed that the roughness increases with increasing doping ratios, which leads to uniform grain geometry that coheres well with each other at doping added.

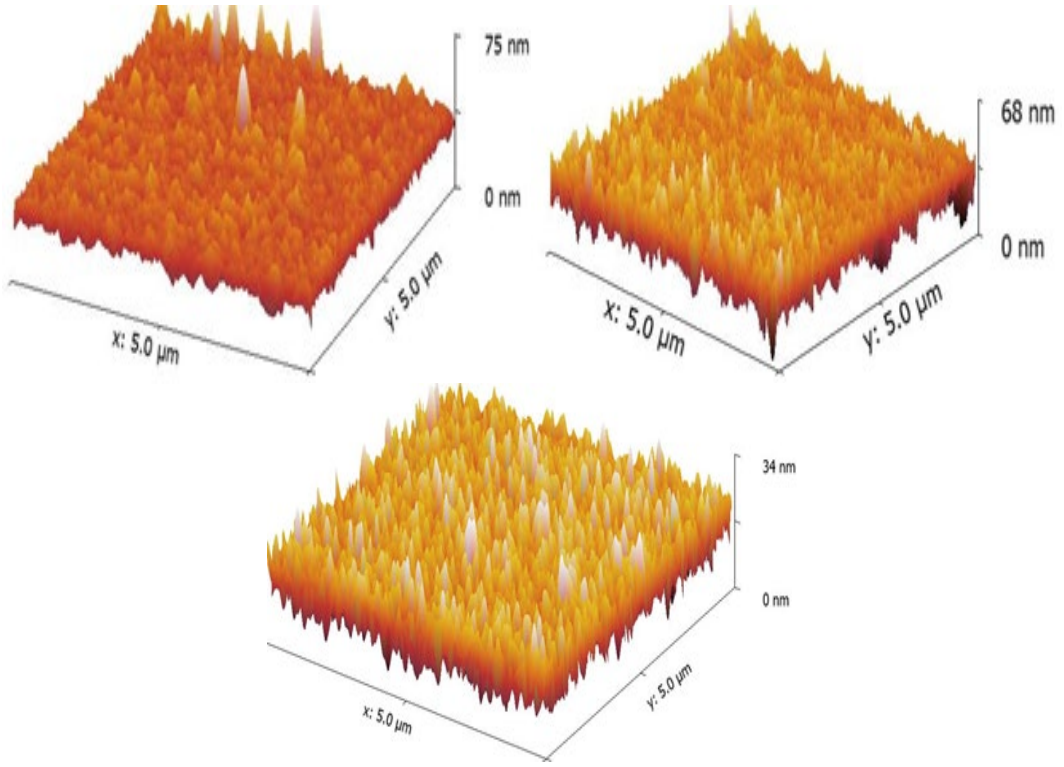

Fig. 3. Shows a 3-D AFM diagram of CuO and CeO_2-doped CuO at (5 and 9%) of CeO_2.

Table 1. AFM parameters for CuO and CeO_2-doped CuO at (5 and 9%) of CeO_2.

CeO_2 %	Average Grain sizes (nm)	Roughness Average (nm)	Root mean square (nm)
CuO	61.4	2.7	3.8
5%	54.8	2.9	4.2
9%	50.3	3.5	4.7

3.3. PL analysis

Fig.4 depicts the photoluminescence (PL) spectra of produced films. The PL spectrum establishes the concept of quantum confinement. It demonstrates that emissions result from (e-h) pair recombination in quantum wells with separated energy levels. These energy levels were created by discrete bulk areas produced by nanocrystal particles. The PL spectrum of the films prepared was highly shifted to short wavelength when compared with the spectrum of the bulk CuO nanocrystal structure as a function of doping ratio, and blue shift is occurring in the PL spectrum. The emission spectrum of pure CuO sample exhibited a distinctive red emission at around 725 nm. Improved luminescence intensity after CeO_2 doping, a blue shift occur in peaks position as ratios increased. This resulted in an increased energy gap because of size reduction because of charge carriers quantum confinement. When compared to the naked substrate, this augmentation signify a good achievement. Table 2 shows how the particles size decreases according to the Brus equation.

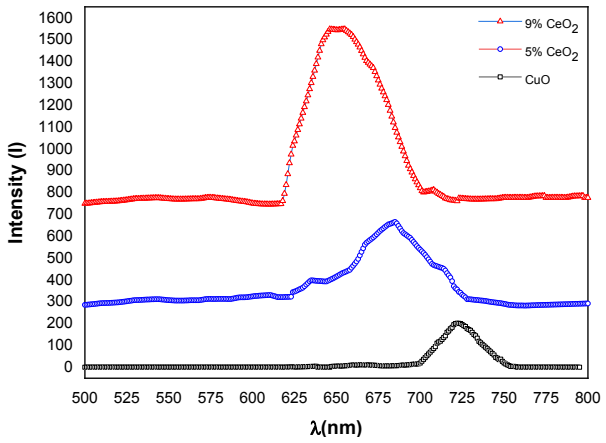

Fig. 4. PL spectra of CuO, and CeO_2-doped CuO at (5, and 9%) of CeO_2.

Table 2. PL parameters for CuO and CeO_2-doped CuO at (5 and 9%) of CeO_2.

CeO_2%	**Wavelength (nm)**	**Intensity (nm)**	**Energy Gap (eV)**	**Particle size (nm)**
CuO	725	205	1.71	22.0
5%	685	650	1.81	19.2
9%	650	1540	1.97	16.4

3.4. Gas Sensor Performance

Fig. 5 indicates the resistance of pure CuO deposited on a non-metallic substrate as a function of time, with the on/off gas valve exposed to 0.5C, 1C, and 1.5C concentrations of NH_3 gas at 100 C. The resistance increases when the gas is out [17]. The figure shows the sensitivity of gas sensor behavior for CuO pure is a weak response. Table. 3 shows the change in the values of sensitivity, response, and recovery time with the change in the concentration of gas.

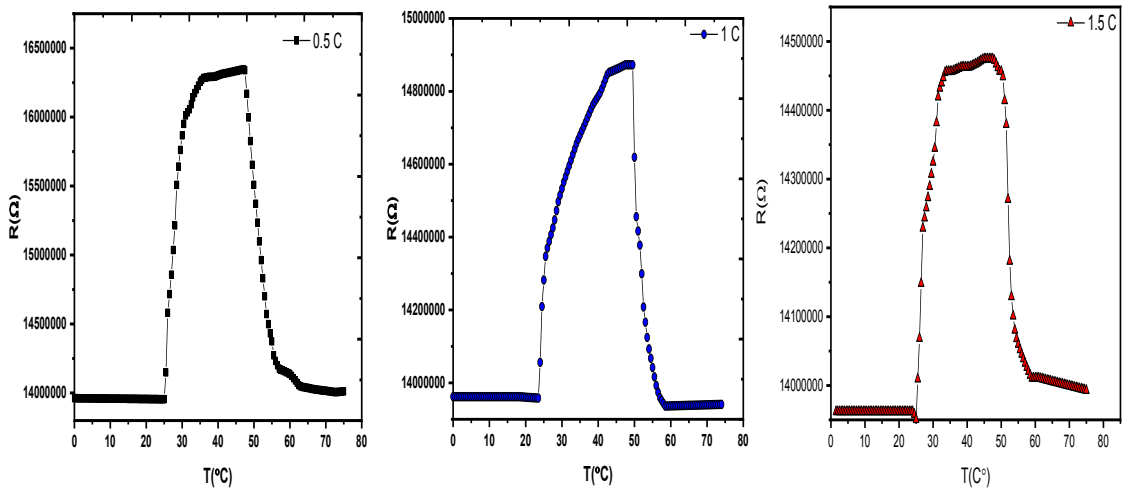

Fig. 5. Resistance as a function of time of pure CuO.

Fig. 6 and 7 show the resistance of the CuO doped with CeO_2 at ratios of 5 and 9% wt. The sensitivity improved significantly due to the catalyst effect of CeO_2 nanoparticles in the structure of metal oxide. These new structures increased the sensitivity of CuO. The results showed an increase in the detection process (sensitivity) with the increase in gas concentration. This is a natural outcome duo to the semiconductor conductivity increases with concentration increased. The amount of NH3 chemically adsorbed on the surface of CuO doped with CeO_2 is more than the amount on CuO. As a result, it was plausible to conclude that finely scattered CeO_2 species were the primary NH_3 adsorption sites, where the adsorption capacity of NH_3 for CuO: CeO_2 was clearly greater than that of CuO and CeO_2 separately. The response and recovery time decrease when cerium oxide is added, as shown in Table 3.

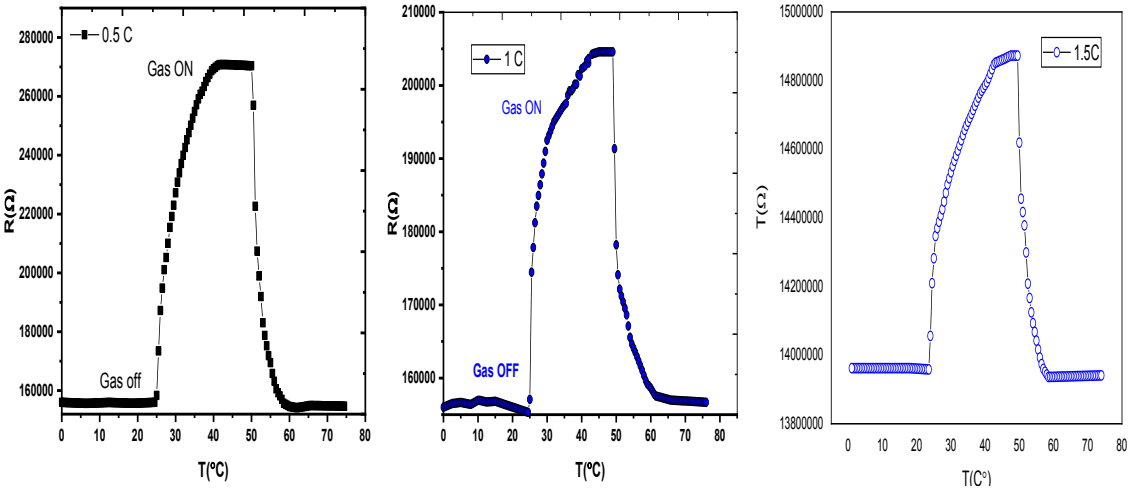

Fig. 6. Resistance as a function of CeO_2 -doped CuO at (5%) for CeO_2.

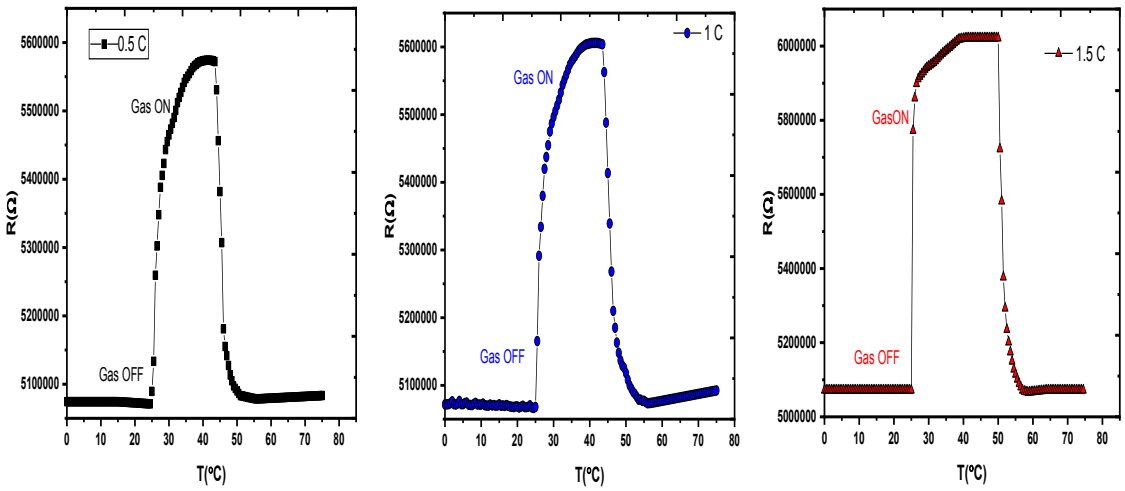

Fig. 7. Resistance as a function of CeO_2 -doped CuO at (9%) for CeO_2.

Table 3. Gas sensor parameter of CuO, and CeO_2 -doped CuO at (5, and 9%) for CeO_2.

Sample	Response time (s)			Recovery Time (s)			Sensitivity S %		
	0.5C	**1C**	**1.5C**	0.5C	1C	1.5C	0.5C	1C	1.5C
CuO	32	31.4	31.1	36.6	32.2	31.9	8	12	18
5% CeO_2	30.2	29.4	29.5	33.0	32.3	31	28	33	38
9% CeO_2	28.7	28.2	26.1	29.5	27.8	27.0	41	46	48

4. Conclusion

In this research, a hydrothermal method was used for the synthesis at copper oxide, and demonstrated an amazing reliance on CeO_2 doping. The CuO nanostructures composite has monoclinic CuO structures, CuO thin sensing according to the XRD study, and the crystalline size decreases as the CeO_2 concentration increases. The grain size at the nanoscale is set by AFM topography, which shows decreases with increasing CeO_2 ratios. The energy gap obtained of PL spectrum increase with increasing doping ratio. According to Brus equation, the particle size decreases as CeO_2 ratio increase. The results showed increasing in sensitivity with increase the doping ratio, and gas concentration, the performance sample toward gas sensitivity was found at 9% of CeO_2, and 1.5 C concentration. The sensitivity of NH_3 gas refer to the moderate response, which increase with doping ratio increases, while the response and recovery time decreased with increasing doping and gas concentration.

References

[1] A. I. Ayesh et al., Appl. Phys. A Mater. Sci. Process., vol. 125, no. 8, pp. 1-8, 2019; https://doi.org/10.1007/s00339-019-2856-6

[2] G. Di Francia, B. Alfano, V. La Ferrara, J. Sensors, vol. 2009, no. May 2014, 2009; https://doi.org/10.1155/2009/659275

[3] S. Steinhauer, Gas Sensors Based on Copper Oxide Nanomaterials : A Review, 2021; https://doi.org/10.3390/chemosensors9030051

[4] O. A. Fahad, A. S. Mohammed, Mater. Today Proc., no. 2, pp. 3-7, 2021; https://doi.org/10.1016/j.matpr.2020.12.547

[5] T. Li, N. Bao, A. Geng, H. Yu, Y. Yang, Subject Category : Subject Areas : Study on room

temperature gas-sensing performance of CuO film-decorated ordered porous ZnO composite by In 2 O 3 sensitization, 2018; https://doi.org/10.1098/rsos.171788

[6] G. Applications and A. Rydosz, The Use of Copper Oxide Thin Films in, 2018; https://doi.org/10.3390/coatings8120425

[7] I. Singh, S. Dey, S. Santra, K. Landfester, R. Muñoz-Espí, A. Chandra, ACS Omega, vol. 3, no. 5, pp. 5029-5037, 2018; https://doi.org/10.1021/acsomega.8b00203

[8] I. M. Ibrahim, " Iraqi J. Phys., vol. 15, no. 35, pp. 64-74, 2018; https://doi.org/10.30723/ijp.v15i35.54

[9] E. Laubender, N. B. Tanvir, O. Yurchenko, G. Urban, Procedia Eng., vol. 120, pp. 1058-1062, 2015; https://doi.org/10.1016/j.proeng.2015.08.729

[10] J. Wang et al., Sensors Actuators, B Chem., vol. 255, pp. 862-870, 2018; https://doi.org/10.1016/j.snb.2017.08.149

[11] Z. Wang, Z. Qu, X. Quan, Z. Li, H. Wang, R. Fan, Appl. Catal. B Environ., vol. 134-135, pp. 153-166, 2013; https://doi.org/10.1016/j.apcatb.2013.01.029

[12] X. Zhang, H. Wang, X. Jiang, H. Sun, Z. Qu, Catal. Sci. Technol., vol. 9, no. 11, pp. 2968-2981, 2019; https://doi.org/10.1039/C9CY00480G

[13] A. Z. Al-Jenaby, A. Ramizy, A.-M. E. Al-Samarai, " IOP Conf. Ser. Mater. Sci. Eng., vol. 1095, no. 1, p. 012006, 2021; https://doi.org/10.1088/1757-899X/1095/1/012006

[14] N. J. Mohammed, Al-Mustansiriyah J. Sci., vol. 29, no. 4, pp. 122-127, 2019; https://doi.org/10.23851/mjs.v29i4.441

[15] G. Li, X. Zhu, X. Tang, W. Song, Z. Yang, J. Dai, J. Alloys Compd., vol. 509, no. 14, pp. 4816-4823, 2011; https://doi.org/10.1016/j.jallcom.2011.01.176

[16] A. Ramizy, A. S. Mohammed, I. M. Ibrahim, M. H. Eisa, Int. J. Nanoelectron. Mater., vol. 13, no. 1, 2020.

[17] A. S. Mohammed, O. Abed, A. Ramizy, E. Yahya, Ceram. Int., no. March, 2021; https://doi.org/10.1016/j.ceramint.2021.03.103